Dissociation Mechanisms of G-actin Subunits Govern Deformation Response of Actin Filament

Sharad Jaswandkar, H M Nasrullah Faisal, Kalpana S. Katti, Dinesh R. Katti*

Department of Civil and Environmental Engineering,

North Dakota State University, Fargo, ND 58105, USA

* Corresponding author, <u>Dinesh.Katti@ndsu.edu</u>. 701-231-7245

ABSTRACT

The actin molecules are essential structural components of the cellular cytoskeleton. Here, we report a comprehensive analysis of F-actin's deformation behavior and highlight underlying mechanisms using steered molecular dynamics simulations (SMD). The investigation of F-actin was done under tension, compression, bending, and torsion. We report that the dissociation pattern of conformational locks at intra-strand and inter-strand G-actin interfaces regulate the deformation response of F-actin. The conformational locks at the G-actin interfaces are portrayed by spheroidal joint, interlocking serrated plates analogy. Further, the SMD simulation approach was utilized to evaluate Young's modulus, Flexural rigidity, Persistent length, and Torsional rigidity, of F-actin and the values obtained, were found to be consistent with available experimental data. The evaluation of the mechanical properties of actin and the insight into the fundamental mechanisms contributing to its resilience described here are necessary for developing accurate models of eukaryotic cells and for assessing cellular viability and mobility.

KEYWORDS: Actin filament, Molecular dynamics, Steered molecular dynamics, Mechanical properties, Loading paths.

1. INTRODUCTION

The cytoskeleton's dynamic structure is a network of interlinking protein filaments, helping the cells maintain their shape and internal organization. Actin filaments (F-actins) are linear polymers of globular actins (G-actin subunits) act as an essential structural member of the cytoskeleton in eukaryotic cells.^{1, 2} The globular protein G-actin consists of 375 amino acids. Each F-actin subunit (G-actin) has stable binding sites that mediate their head-to-tail interactions with two additional subunits. Since all the G-actin subunits are aligned in the same direction, actin filaments have a definite polarity, and their ends are differentiable from each other (barbed (+) and pointed (-) ends).³ F-actins can form different morphologies, such as actin bundles and cross-linked networks.⁴ The different actin morphologies play a crucial role in various cellular processes, including motility, mitosis, cellular polarity, and embryogenesis.⁵ Several serious diseases such as muscle disorders and cancer have been linked to dysfunction of the actin network and focal adhesion proteomes. 6-10 The vital role of F-actins in performing cellular functions depend on their mechanical responses/properties.^{2, 11} Hence, an in-depth understanding of F-actin mechanics is essential to understand how the actin cytoskeleton aids cells' biological functions. Previous research studies on the mechanical properties of F-actin can be divided into two related scopes: experimental and modeling-based investigations. Fujime performed the first empirical study of Factins' mechanical properties. 12 A sequence of developments continued with the experimental techniques used to understand F-actin's thermal fluctuation, such as optical fluorescence microscopy¹¹ and optical/electron microscopy. ¹³⁻¹⁵ Simultaneously, new technologies have also been documented for measuring F-actin's mechanical properties, to mention a few, fluorescence microscopy, ¹⁶ optical tweezers, ^{16, 17} rheometers, ¹⁸ atomic force microscopy, ^{19, 20}. The extensional stiffness of 1 µm length F-actin was measured using direct nanomanipulation. 21 In

vitro micromanipulation study has also been conducted to examine the torsional rigidity of Factin.²² Additionally, several prior studies are also focused on computer simulation; these studies can be divided into three major classes: molecular dynamics (MD) simulations, multiscale modeling, and continuum mechanics modeling. MD simulations have been found to be effective in F-actin structural modeling.²³⁻²⁵ Further, MD simulations also helped shed light on F-actin's elastic properties. 26-29 In analyzing the mechanical properties of F-actin, Coarse-Grained MD simulations have been found to be satisfactory.³⁰ To explore the biomechanical properties of Factin networks, a multiscale hierarchical model was developed.³¹ Besides, some experimental studies were also performed to understand actin mechanics. Few findings reported that the actin endures much higher stresses than other cytoskeletal members but starts to rupture and flow at a strain of about 20%. 32 Cyclic tensile forces on actin filaments induces dramatically improved Gactin-G-actin bond lifetime and different kinetics of dissociation.³³ Actin bundles exhibit a frequency-dependent bending rigidity behavior.³⁴ The F-actin bundle is strong and rigid to bend along the long axis.¹⁷ Conformation changes are triggered by the mechanical stress applied to an actin filament, modifying actin-binding proteins' binding and regulatory action. 35, 36 By extending bond lifetimes, the G-actin-G-actin and G-actin-F-actin dissociation kinetics, are regulated by tensile force.³⁷ The F-actin's torsional twist is involved in the development of the filopodial actin mediated force.³⁸ For cross-linked networks, F-actin stretching regulates deformation dynamics, leading to a stress-stiffening regime and an extremely tunable response to deformation.³⁹ Although several modeling studies have been conducted in the literature to study the mechanical properties of F-actin, very little research has been performed that focuses on investigating the underlying mechanisms governing the deformation response of F-actin. Previous work from our group on mineral-protein interaction, deformation behavior of collagen, investigation on mechanical properties of montmorillonite interlayer using MD simulation have provided an insight into the mechanisms that govern their mechanical properties⁴⁰⁻⁴² enabling unique applications in tissue engineering.⁴³ In this work, steered molecular dynamics (SMD) simulations of F-actin are performed to understand F-actin dynamics and investigate its mechanical properties. Here, the study on F-actin's mechanical response was carried out by four modes of deformation, axial stretching, axial compression, Three-point bending, and torsion. The choice of these loading paths is motivated by forces acting on actin filaments during cell movement or motility.^{4,44-46}

2. MATERIALS AND METHODS

2.1. F-Actin Model Construction and Molecular Dynamics Simulation Details

The PDB coordinates for F-actin were obtained from the Protein Data Bank (PDB) entry 3LUE.⁴⁷ This protein structure was composed of ten subunits of F-actin and ten units of alphaactinin. Since this study focuses on the actin filament, the alpha-actinins are removed from the simulation system. For model simulations with ATP, ATP coordinates from the ATP G-actin PDB entry 1ATN⁴⁸ were used. The F-actin protein structure and coordinate files were generated using the Nanoscale Molecular Dynamics (NAMD) psfgen tool,⁴⁹ using topology, and force-field parameter files from Harvard Molecular Mechanics (CHARMM).⁵⁰ Using the VMD plugin to solvate (the TIP3P force field for the water model), the F-actin molecule was placed in a water box. Next, the system was brought to electrostatic neutrality using the VMD autoionize feature. The NAMD software⁵¹ and the CHARMM36 force fields were used to conduct all simulations. The energy minimization of the molecule was carried out by the conjugate gradient method. The temperature and the pressure of the molecule were increased to 300 K and 1.01325 bar, respectively, in incremental steps of 100 K and 0.25 bar. Langevin dynamics, Nose-Hoover

piston methods were adopted to control temperature and pressure.^{52, 53} The minimized and equilibrated structure was the starting point for all simulations. The F-actin stability without an applied load was verified by the root mean squared deviation data obtained from the trajectory of molecular dynamics.

2.2. Steered Molecular Dynamics (SMD) Simulation Details.

The SMD simulations for tension, compression, and bending tests were performed at constant velocity using the NAMD implemented approach.⁵¹ The tension and compression tests were carried by fixing one end (by applying constraints) and applying pull or push on the center of mass of the terminal G-actin subunits utilizing harmonic spring of fixed spring constant. The strain rates used in tension and compression simulations were 0.0002, 0.0004, 0.0005, 0.0006, 0.0008 ps⁻¹. The spring constant's optimum value was chosen by running tension test simulations for different spring values (refer to supplementary information). Based on the results, a spring constant of 9 kcal/mol/Å² was chosen. The bending test simulation was performed by fixing both ends of the filament and applying load at the midpoint in a transverse direction. The displacement velocities used in bend tests were 0.06, 0.12, 0.14, 0.18, 0.25 Å/ps. The torsion test on a filament was carried out using user-defined forces in the SMD simulation (refer to supplementary information). During simulations, different values of torque were applied on one end, keeping another end fixed. The torque values used for simulations were 425, 850, 2125, 4250 pN-nm. The lower to higher range values of torque was used to verify the torsional rigidity of filament. All the simulations were performed using a 0.5 fs time step. For all nonbonded interactions, a cutoff distance of 10 Å was used. In the development and stabilization of protein structures, hydrogen bonds (H-bonds) play a crucial role. Here, for all simulations, hydrogen bonds' evolution was analyzed using a combination of geometric parameters (donor hydrogen distance limit 3.5 Å and donor hydrogen acceptor angle $\leq 30^{\circ}$). The initial length of F-actin is L₀ (31 nm) was estimated by measuring the distance between the center of mass of the terminal G-actin subunits, and the cross-sectional area (A) was estimated by equation $A = \frac{\pi}{4} d^2$, where d is the diameter of F-actin, d = 7 nm. For each value of strain rate/displacement velocities/torque, the simulation was repeated four times. All the graphs presented and mechanical properties calculated were obtained from averaging results from all simulations. For a detailed description of the different terms used in this study, please refer to supplementary information.

3. RESULTS AND DISCUSSION

F-actin consists of two strands, which gradually turn around each other to form a two-strand right-handed long helical structure. Along the helix axis, the G-actin molecules are situated at an incremental distance of around 27.6 Å and angular separation of $166^{\circ} \pm 6^{\circ}$. Thus, the helical F-actin structure results from G-actin molecules' systematic geometric conformity, held together by nonbonded interactions. S5, S6 Such a system facilitates the assembly and rapid disassembly of actin filaments in response to biochemical or mechanical signals. In this paper, the helix of individual strings is denoted as a strand n and strand n'. In addition, the contacts between neighboring G-actin subunits within a strand (n or n') are named as intra-strand (axial) G-actin interactions, and the contacts between adjacent G-actin subunits, one of them from strand n and another from strand n' are named as inter-strand (helical) G-actin interactions.

3.1. Extensional Deformation.

In this section, the extensional behavior of F-actin was examined by applying a tensile force. The force-extension curves corresponding to different pulling rates are presented in Figure 1a. The unique pattern of F-actin's strain response can be separated into three regimes: stress stiffening, stress softening, and steady-state rupture. Here, the wavy stress-strain response sharply increases to its maximum limit in a strain range of 0 % to 8%, and then, it starts dropping slowly until it reaches a 20 % strain. Furthermore, in the third regime, the F-actin continues to elongate beyond 20% strain, nearly at constant mean stress. The third regime indicates failure at almost constant stress conditions, which is in alignment with what was previously observed in an experimental study.³² Actin filaments change the rigidity according to the loading rate, amplitude, and the nature of the load. 57, 58 Previous studies on reconstituted actin networks also emphasized the stress-stiffening propensity of F-actin in response to axial tensile loads.^{57, 59} Further for Factin, the relationship between force and extension is sensitively dependent on the degree of an extension, and with increasing extension, the tensile force diverges nonlinearly. 60-62 Results supporting these investigations have been found here. Our findings have also shown that the stressstrain curve's form considerably changes from lower to higher strain rates as the strain rate increases. The peak tensile stress was increased along with a slight rise in an elastic modulus (Figure 1b), from lowest to highest strain rates. However, strain to failure decreased with increasing strain rate (Figure 1c).

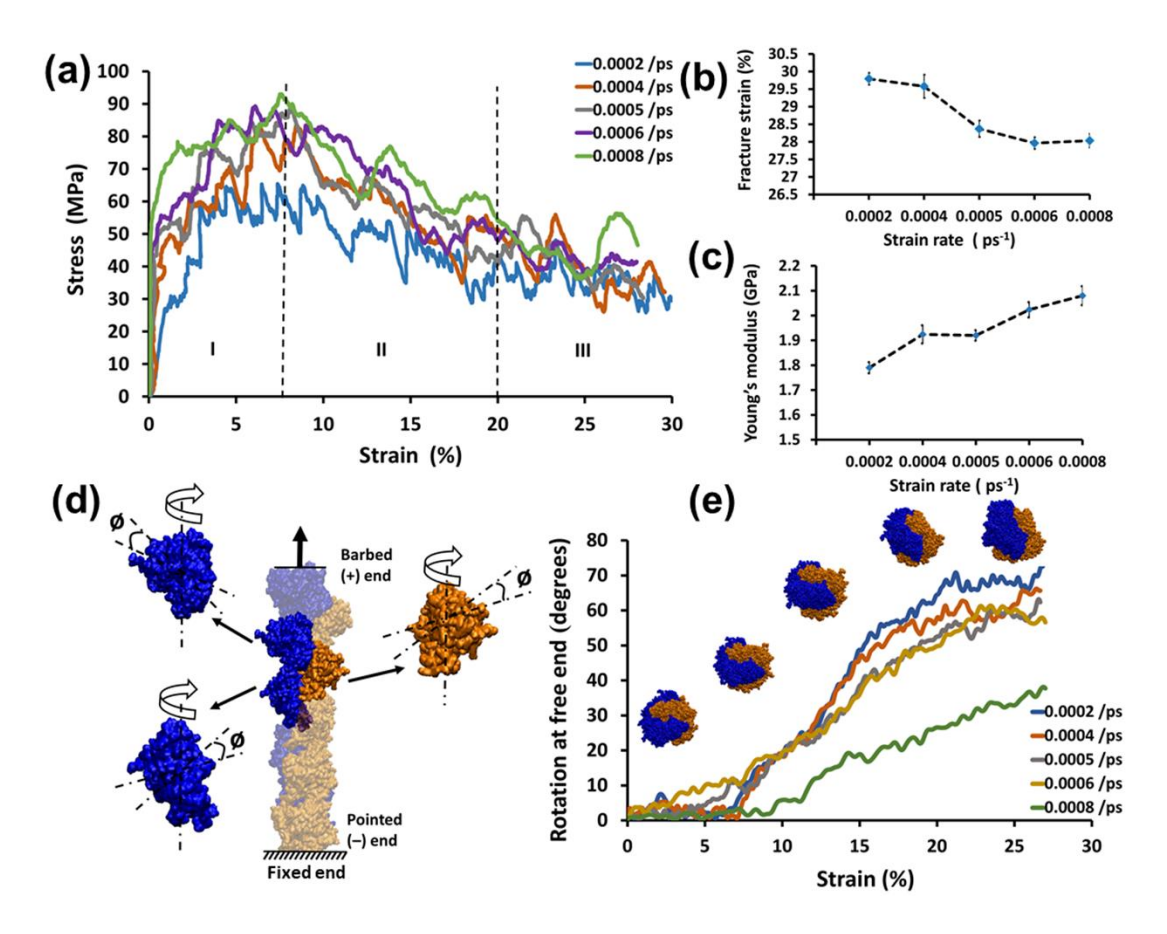


Figure 1. Strength, Fracture strain, Young's modulus, Angular displacement as a function of strain rate. The results of tensile test simulations are presented here. (a) The strain-rate dependence of the tensile response of actin filament is separated into three regimes: stress stiffening (I), stress softening (II), and steady-state rupture (III). Higher pulling rates led to a stiffer response of F-actin and thus greater strength. (b) Variation of fracture strain as a function of strain rate. The plot shows a decrease in fracture strain in response to higher pulling rates. (c) Young's modulus is represented as a function of strain rate. (d) The atomic structure of F-actin with pointed (-) end fixed and subjected to tensile load on the free end (barbed (+) end). It represents how the free end rotation is linked with turning (ø degrees) of G-actin subunits along the filament's longitudinal axis. (e) The tensile force caused the rotation of the free end. Here, we captured the rotation of the free end (observed from the barbed end) of F-actin during extension at various strain rates.

The elastic modulus calculations were done by using the equation for Young's modulus, Y = $k_{F-actin} \times {}^{L_0}/_{A}$. 63, 64 In this equation, the initial length of F-actin is L₀, and the cross-sectional area is A. The stiffness of F-actin, $k_{F-actin}$ was estimated by the least-square linear fit of loaddisplacement plot up to 5 % strain. Here, the average Young's modulus obtained was 1.95 ± 0.15 GPa, in good agreement with the value of 1.3-2.5 GPa reported in the available experimental studies. 15, 21, 65, 66 The helical structure of F-actin implies that twisting and stretching must be interrelated, hence during stretching, we have observed substantial unwinding of the free end of F-actin (Figure 1e). The elongation of F-actin causes rotation of G-actin subunits along the longitudinal axis as effect free end gets rotated.²⁸ The rotation of the free end is found to be dependent on the extent of elongation and the strain rate-driven varying magnitude of rotation of G-actin subunits along the longitudinal axis of the filament. With increasing tensile force and the F-actin elongation beyond 7-10 % strain, the filament's free end starts to rotate rapidly, as shown in figure 1e. It is observed that the elongation causes a change in F-actin structure; as a result, depending on the conformational arrangement and adjacent interaction, G-actin subunits acquire new positions. The observed rotation (ø) of G-actin subunits was strain rate dependent and varied in the range of 3° to 7° per subunit. The elongation at high strain rates results in rapid conformational transition in the F-actin structure; as a result, G-actin subunits do not get sufficient time to rearrange, which resulted in lower rotation of the free end.

We have observed that F-actin's stretching arises from the deformation of F-actin subunits (G-actins) and displacement of G-actin-G-actin interfaces. We also observed that the F-actin's deformation response in the first region resulted from a direct extension of intra-strand G-actin-G-actin atomic interactions (axial interactions). Whereas in the subsequent region, displacement of inter-strand G-actin interfaces dominates. Figure 2a captures those characteristics by displaying

the atomic scale elongation process as a function of the percentage of strain and confirms the connection of F-actin elongation response with the G-actin-G-actin dislocation mechanism. Here, the two strands of actin filament are represented by strand n (Blue) and n' (Orange), and G-actin Subunits are labeled in consecutive number sequence from the barbed (+) end.

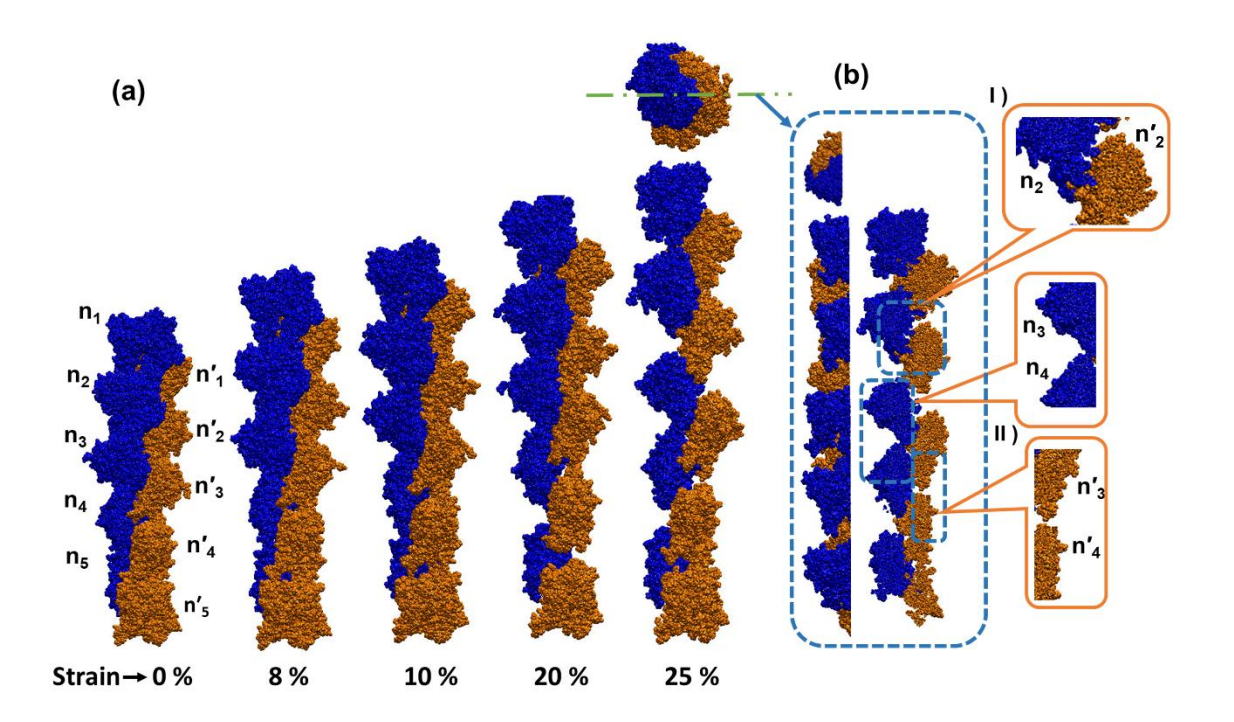


Figure 2. | SMD simulated F-actin labeling conventions and a conformation transformation under tensile force.

(a) Double-stranded helical structure marked as strands n (blue) and n' (orange) and G-actin subunits are labeled in a natural numbers sequence from barbed (+) end. The nature of the sliding of conformational locks at G-actin-G-actin interfaces in axial directions while stretching of the filament depends on the degree of the elongation. Snapshots are demonstrating patterns of force-induced deformation. Initial structure (0 % strain), the structure at 8 %, 10% 20%, 25% strain (b) Cross-sectional view along the section line (Green) captured to get a detailed insight into actual intrastrand and inter-strand G-actin connections in an actin filament (recorded at 25 % strain).

The reason for the jagged nature of the stress-strain curve was investigated, and it appears that this response is the result of the subunits of the F-actin (G-actins) sliding over each other while

stretching. This sliding process occurs in a discontinuous way due to the atomically rough contact surface of nonbonded interactions and patterns of formation of the hydrogen bond. Figure 3 captures those features by presenting a precise record of the change in the number of hydrogen bonds within the F-actin and the change in the number of hydrogen bonds at intra-strand, interstrand G-actin interfaces as a function of the elongation, estimated by strain. For all the strain rate spectrum, we detected a decrease in the total number of hydrogen bonds within F-actin of about 17 ± 0.21 H-bond / nm before 15% strain, and the number of hydrogen bonds becomes 29 ± 0.13 H-bond / nm beyond 15% strain (Figure 3b).

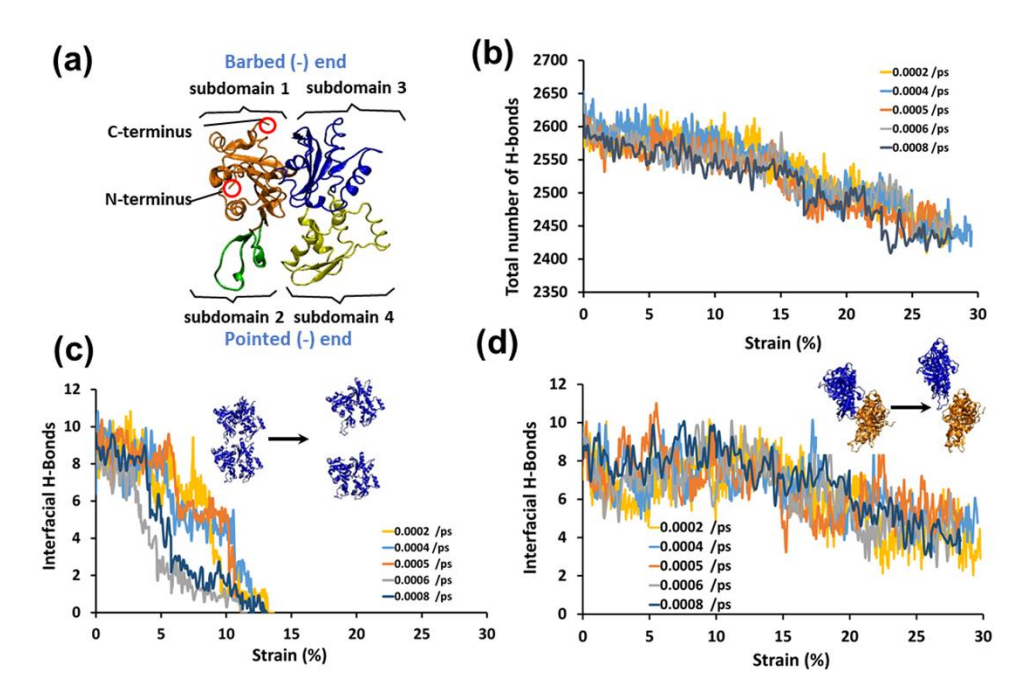


Figure 3. | Three-Dimensional Structures of G-actin and hydrogen bonds analysis. (a) G-actin's Domain organization is labeled into four domains. The orientation is represented using convention, the + end (barbed end) at the top, and the + end (pointed end) at the bottom. (b) Show the decrease in the total number of hydrogen bonds in F-actin as a function of strain. (c) Here, we captured a decrease in intra-strand G-actin-G-actin interfacial hydrogen bonds in response to strain. (d) Displays, decrease in inter-strand G-actin-G-actin interfacial hydrogen bonds in response to strain. Snapshots differentiate the G-actin-G-actin hydrogen bonds breaking pattern. Here, hydrogen bonds calculation in graphs c, d is done by averaging the G-actin-G-actin interfacial hydrogen bonds.

We observe that this pattern of decrease in the total number of the hydrogen bonds resulted from the unfolding of intra-strand G-actin-G-actin conformational locks, mediated by breaking of the hydrogen bonds and shifting of inter-strand alignment in the direction of applied tension. We can understand this phenomenon from figure 2a; upon stretching, the G-actin subunits in a strand start separating, and they dissociate entirely at 10-12 % strain. As a result, the breaking of hydrogen bonds at intra-strand G-actin-G-actin interfaces occurs rapidly within a 0-12 % strain range (Figure 3c). However, stretching also results in the sliding of G-actin subunits at interstrand interfaces, which give rise to an exclusive pattern of variation in hydrogen bonds as a function of strain (Figure 3d). Here, there was not much variation in the number of hydrogen bonds within the strain range of 0-12%, indicating continuous breaking and reformation of the Hbond; further, the number of hydrogen bonds decreased slowly beyond 12%. This sliding of interstrand G-actin-G-actin interfaces continues until the filament ruptures. The hydrogen bond breaking patterns observed here may lead to the force-dependent catch-slip bond formation observed in experimental studies conducted on F-actin.³⁷ Further, studying the transition of energy while stretching revealed that the energy at G-actin-G-actin interfaces consisted mainly of electrostatic energy. F-actin's energy changes in the SMD simulation are shown in figure 4. It shows a similar trend that has been observed in hydrogen bond analysis. The energies at intrastrand G-actin-G-actin interfaces reduced as strain increases and became zero at around 15 % strain (Figure 4a-b). However, it gradually reduced at the inter-strand G-actin-Gactin interfaces. Actin filament bundles and networks are cytoskeletal high-order structures consist of actin filaments bind with various actin-binding proteins. Hence, their deformation response mostly depends on the size, orientation, and arrangement of the constituents.⁶⁷ However, since these fibrous structures mainly consist of actin filaments, their response to the applied force is

strongly influenced by F-actin mechanics. Therefore, the deformation mechanics of single actin filament presented here is crucial to understand their high-order/bulk structural behavior.

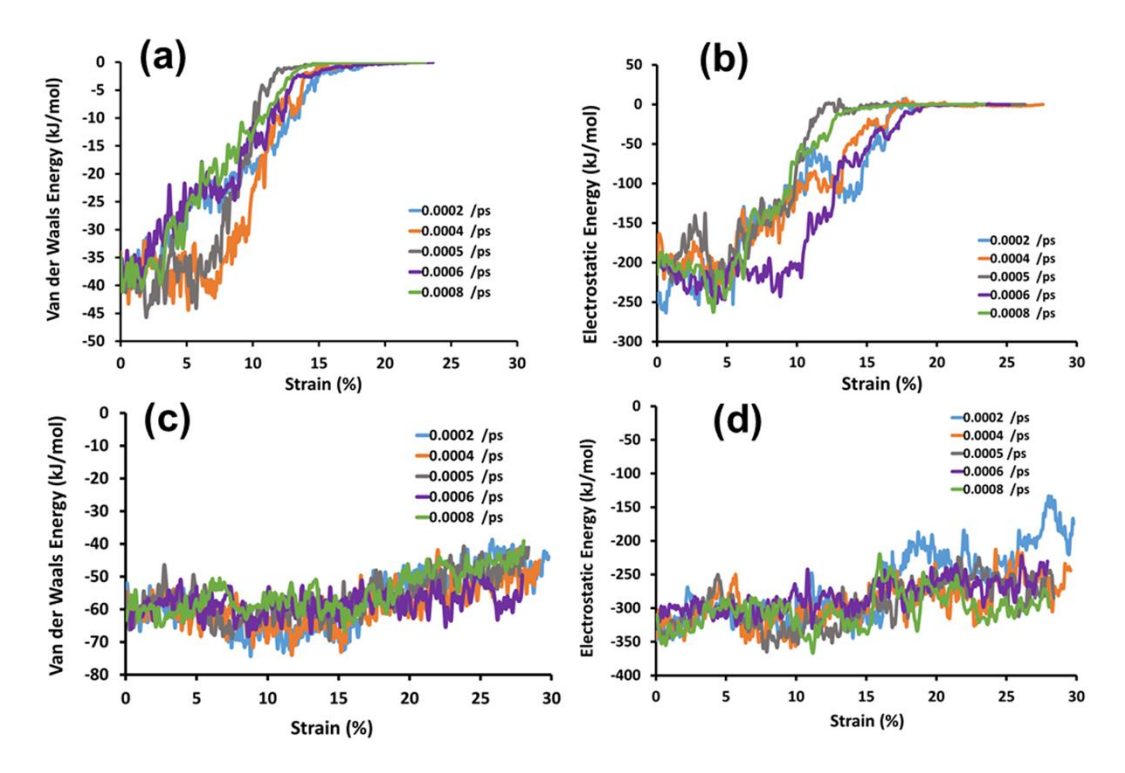


Figure 4. Changes in the interaction energies at G-actin interfaces. Displacement of G-actin subunits during elongation of F-actin resulted in changes in the interaction energy at G-actin interfaces. (a-b) Variation in Van der Waals and Electrostatic energy at intra-strand G-actin interfaces plotted as a function of strain. (c-d) Curves demonstrate variation in Van der Waals and Electrostatic energy at inter-strand G-actin interfaces in response to strain. Here, energy calculation is done by averaging the energies G-actin-G-actin interface.

3.1.1. Contact between F-actin subunits and pulling force-induced generation of new Interactions.

The structure of a G-actin consists of four subdomains (Figure 3a). The subdomains 1, 3, and 4 have well-defined hydrophobic cores and act as stiff, independent units on G-actin-to-F-actin transformation.⁶⁸ An exception to this is Domain 2; in domain two, a structure called the D-loop is located between the residues of 40 (His) and 48 (Gly). This D-loop conformation depends

entirely on the molecule to which it connects. The intra-strand interactions among F-actin subunits (G-actins) appear to be strong along the strands. These features are captured in figure 5a; the spiky projection of residue 238-295 of subunit n₂ is enveloped by residue 37-50, 61-65, 200-208, and 241-247 of subunit n₁, mimicking ball and socket joint (spheroidal joint) like assembly (Figure 5c). Furthermore, D-loop (38-48) of subunit n_1 is outstretched towards the bottom cavity of subunit n₂ between subdomains 1 and 3 and forms noncovalent bonds with subdomain 3 of subunit n₂: Val 45-His 371, Lys 61-Glu 167, and Ile 64-Tyr 166. Domain 4 of subunit n_1 was also in direct contact with domain 3 of subunit n_2 , which forms a few bonds: Asp 244-Arg 290, Gly 245-Ser 323, Glu 205-Asp 286, and Glu 241-Thr 324 (Figure 5b). The axial interactions are, therefore, mainly electrostatic and hydrophilic.⁵⁴ However, the inter-strand interactions are formed by wavy projection, as shown in figure 5d-e. The N-terminal of the alpha helix of (109-116) of subunit n₂ establishes close contact with the C-terminus of an alpha helix (109-199) of subunit n'₁. Further, the hydrophobic plug 265-271 in subunit n₂ forms multiple contacts with opposite strand subunits, including residue 39-42 and 201-203 in subunit n'₁ and residue 285-287 and 169-174 of subunit n'₂. Taking all these into account, the interactions among actin subunits are mostly electrostatic and hydrophilic.⁵⁴

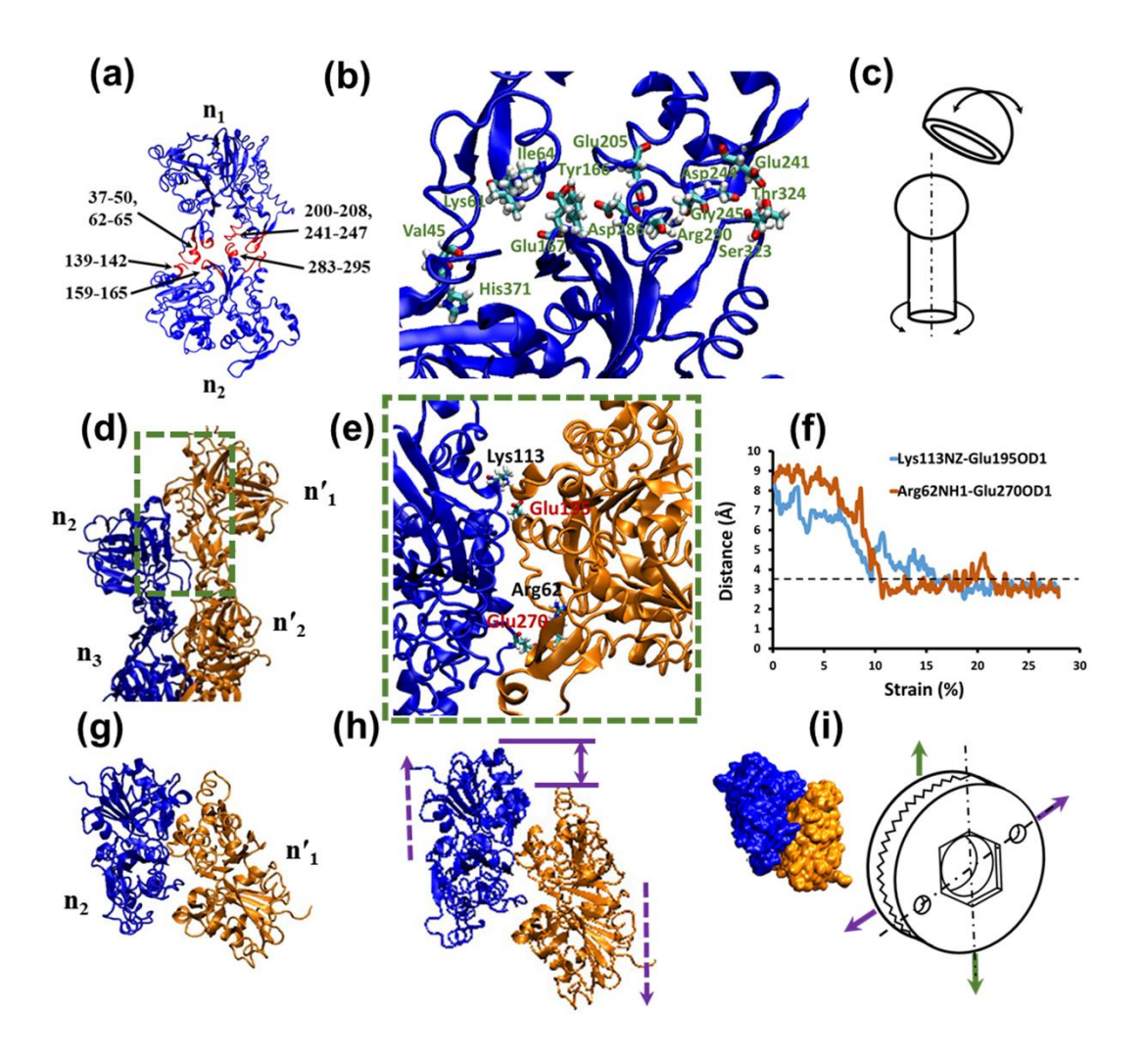


Figure 5. Snapshots of Intra-strand and inter-strand connections within the F-actin model. (a) Snapshot showing the nature of intra-strand G-actin-G-actin contact. Residues involved in contact formation are highlighted (red). Residues of n₁ cover the spikey projection of subunit n₂. (b) Magnified view of Intra-strand contact and relevant residues in stick representation. All stick representations Colored depending on the element: hydrogen-white, oxygen-red, carbon-cyan, nitrogen-blue. (c) Schematic of the ball in a socket analogy. The ball represents a spikey projection of a subunit n₂, and the socket represents the envelope formed by a subunit n₁. (d) Inter-strand interactions in front view. Box represents interface under focus (e) Magnified view of the interface under observation. Elongation caused the sliding of G-actin subunits at the interfaces, which induced new interactions between acidic (red) and basic (black) residues, which were far from each other before pulling. (f) The distances between the salt bridge forming residues are plotted in response to strain. Before pulling, interactions were absent (0 % strain); however, noncovalent

interactions developed when pulled. The graph shows a reduction in interatomic distances below the 3.5 Å limit (dashed horizontal line). (g) Inter-strand interactions were observed in the top view at 0 % strain. (h) Displacement of the inter-strand interface (at 25 % strain) when observed in top view. (i) Snapshot of inter-strand G-actin connection compared with the schematic of the serrated locking plates analogy. The notched edges of plates are analogous to the wavy inter-strand interfaces observed in figure e-g.

The proteins present in all species are made up of 20 amino acids.⁶⁹ In a list of 20 amino acids, three amino acids, Arginine (Arg), Lysine (Lys), and Histidine (His) have basic side chains (+ve charge), and Two amino acids, Aspartate (Asp) and Glutamate (Glu) have acidic side chains (-ve charge). Salt bridges are formed in proteins if oppositely charged residues come close enough (4 Å or less) in a neutral environment. 70 Among the inter-strand interactions, Pulling induced a relative sliding, which enabled new connections. For example, at the inter-strand G-actin-G-actin interface, salt bridges were observed to form between Lys113: Glu195 and Arg62: Glu 270 (Figure 5e-f). These new connections strengthened inter-strand G-actin subunits bonding and could be responsible for strain rate dependent adaptive response of F-actin. Figure 5g-h captures the top view of the inter-strand G-actin conformational lock at 0 % strain and the 25 % strain, respectively, establishing the existence of relative sliding of G-actin in the transverse direction. Here, conformational locks formed by the wavy interface resisted the relative sliding, which led to an elongation of G-actin subunits in the transverse direction (shown by arrows). These conformational arrangements at inter-strand interfaces mimic the serrated locking plates like assembly (figure 5i). Here, the notched edges of serrated plates are analogous with spikey projections at the inter-strand interfaces (figure e-h), establishes the interlocking joint between the G-actin subunits. The serrated locking plates, like contact between G-actin subunits, resulted in resistance to their relative

movement in both longitudinal and transverse directions offering resistance to F-actin against deformation.

3.2. Axial Compression Caused Buckling of Filament About its Weak Axis.

Filopodia are 0.1–0.2-µm diameter rod extensions that act as antennas for cells to monitor their environment. The protrusive bundles in filopodia are made of F-actins. During cell motility, the growth of F-actins generates force for protrusion of the leading edge. The upper limit of force generated for protrusion depends on the critical buckling load of F-actin bundles. The Hence, to explore F-actin's buckling behavior, here, the SMD is used to apply compressive forces at different loading rates to the F-actin. Figure 6a shows how compression simulations are set up and show snapshots of the F-actin deformation profile under compression (snapshots captured for 0.0006 /ps strain rate). Although the F-actin structure appears to be symmetric and circular at all cross-sections, some weak axis sections are based on the initial configuration due to the G-actin subunit's asymmetric shape. The weak axis sections are the regions with a lower moment of inertial, hence less resistant to buckling. We found that failure occurs when the structure buckles in response to a randomly "weakened" axis due to disturbances induced from the heterogeneous evolution of the F-actin's configuration under compressive force. Stress-strain curves for various loading rates are shown in Figure 6b.

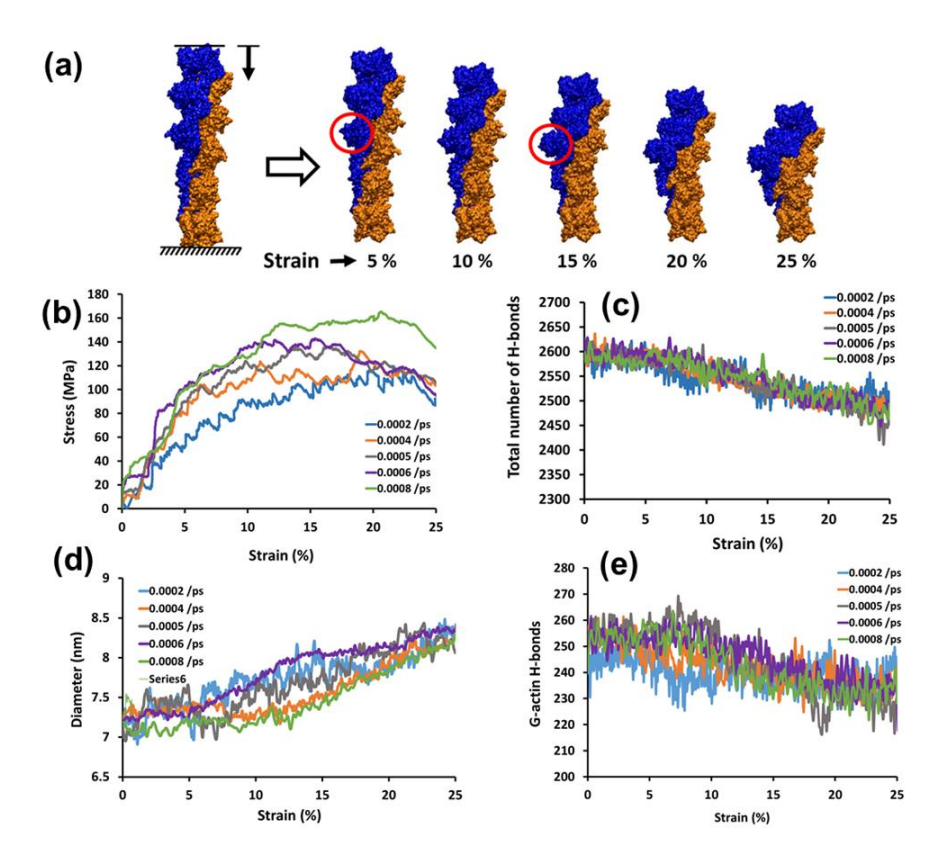


Figure 6. Visual representation of deformation profile and strength, hydrogen bonds analysis as a function of strain rate. (a) The atomic structure of F-actin with one end fixed and subjected to compressive load at the free end. It shows a visualization of the F-actin buckling process, with snapshots taken for different strain values. The highlighted region (red circle) captures bulge formation at 15 % strain, indicating G-acting starts to slip out during the compression process. (b) The strain-rate dependence of the compression test response of actin filament. (c) The decrease in the total number of hydrogen bonds within an F-actin as a function of strain. (d) The average change in diameter of F-actin at various compression rates. (e) The compression causes considerable deformation of G-actin subunits, which resulted in the breaking of hydrogen bonds within G-actin subunits (calculations are done by averaging the H-bonds within G-actin subunits).

The stress-strain behavior displayed a linear elastic regime accompanied by a nonlinear response approaching failure (buckling), similar to observed buckling curves for most engineering materials. In the stress-strain curve, the peak force obtained for each simulation describes an

increase in an F-actin's buckling strength with an increase in applied strain rate, establishing a clear correlation of the compressive stiffness of filament to the strain rate. Further, It is observed that the compressive strength of F-actin is substantially higher than the tensile strength. Hydrogen bond analysis (Figure 6c) shows a rapid decrease in the total number of hydrogen bonds when Factin starts buckling (beyond 10 % strain). The maximum buckling force obtained from simulations associates with the point to which the number of H-bonds in the filament starts to decline, resulting in structural instability. The extended tip of the longest F-actins in filopodia in contact with the barrier only resists the axial compressive load.⁷³ The present work also confirms the short length F-actin's ability to carry the axial compressive load, which is crucial while performing various actin cytoskeletal functions. The results obtained from the simulation determine that the compressive load on F-actin causes significant axial compression of the G-actin subunits, which resulted in the deformation of initial G-actin configurations. The deformation of G-actin configurations causes the breaking of internal hydrogen bonds ((Figure 6e) and an increase in the diameter of F-actin (Figure 6d). To summarize, F-actin's ability to carry axial compressive load arises from hydrogen bond mediated resistance to deformation of G-actin subunits and sliding mechanism at G-actin interfaces. Considering the load-displacement plot up to 10 % strain, the average compressive modulus obtained was 1.62 ± 0.18 GPa.

3.3. Bending Induces Compressive and Tensile Stresses in a Filament.

The flexural rigidity is a structural property of F-actin that measures its ability to withstand bending deformation. The three-point bending test is one of the standard procedures for performing bending tests to obtain flexural rigidity. Here we have used an SMD simulation approach to perform a three-point bending test on the filament. To perform the test, we fixed both F-actin's ends by

applying harmonic constraint on the terminal G-actin subunits (Figure 7a). Next, we selected the midpoint and forced it to move at constant velocity in a direction perpendicular to the F-actin's longitudinal axis to a maximum deflection of approximately 7 nm (Figure 7c).

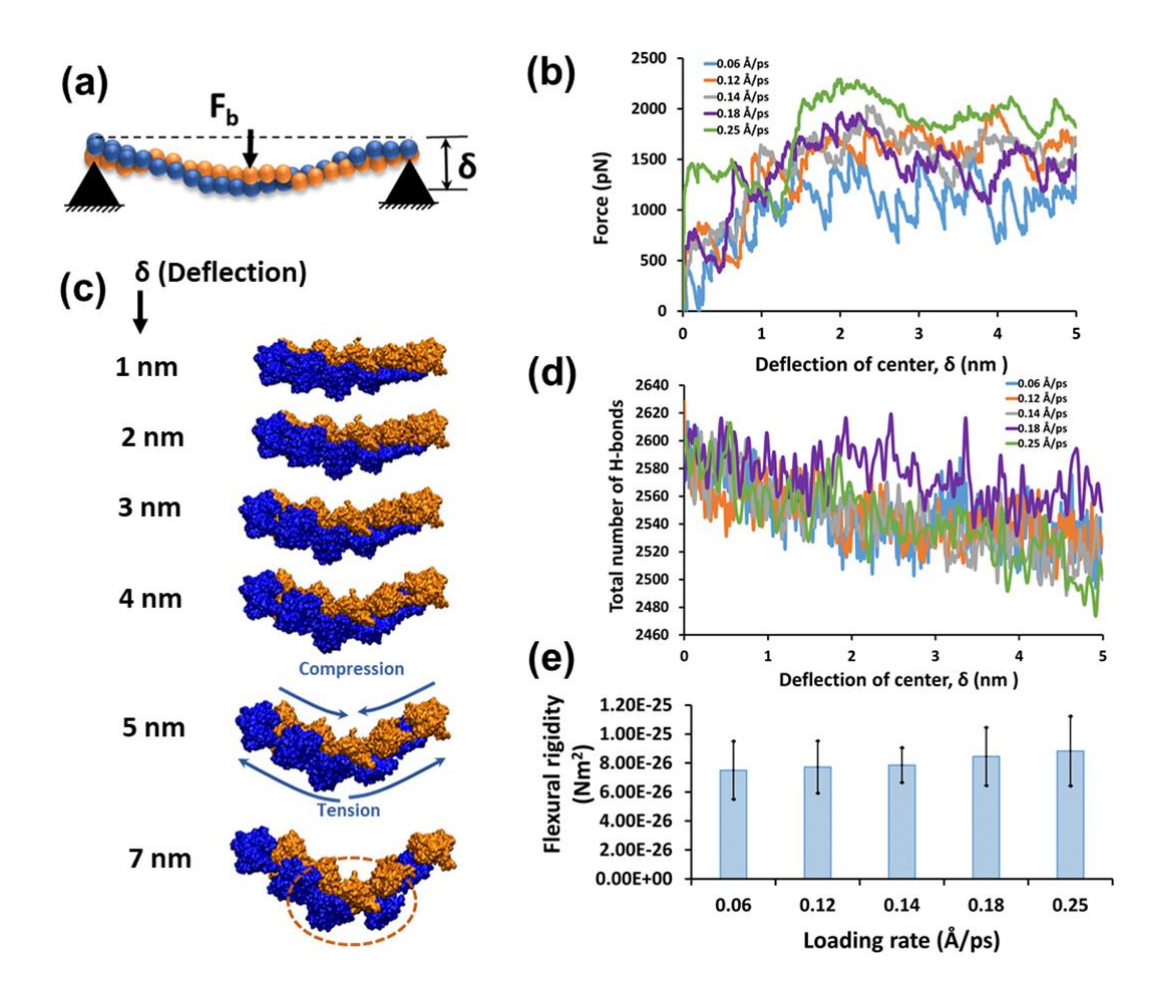


Figure 7. Schematic representation of the bending test with deformation response recorded at various loading rates. (a) Graphical representation of the bending test setup. Here, the F-actin is placed in the horizontal position with ends fixed and subjected to point load at the center. (b) Force displacement curve demonstrating the bending response of F-actin. (c) Images are showing bending deformation of F-actin with an increase in deflection. The filament starts to break on the tension side among the tension and compression sides, as shown by the circle (orange). (d) Change in the total number of hydrogen bonds in F-actin. (e) Flexural rigidity is plotted as a function loading rate.

The setup presented here closely mimics the bending deformation of F-actin in a cytoskeleton environment. Bending of F-actin resulted in a concave curvature shaped deformation. As a result, the top region G-actin subunits are compressed, while lower region G-actin subunits are stretched (Figure 7c). This deformation pattern caused the stretching of G-actin subunits in tension along the longitudinal axis and reflected in the distortion of G-actin interfaces (Figure 7c-d). As a result, the number of hydrogen bonds in F-actin decreases.

The flexural rigidity (product EI) is essential for any bending calculations, where I is a moment of inertia depends on the geometry, and E is Young's modulus of elasticity. From the force-displacement results (Figure 7b), the Bending rigidity (E×I) can be expressed by equation = $\frac{Fl^3}{48\delta}$, where F is the force applied, l is the effective length of the filament, and δ is the deflection (here, the linear regime of bending displacement up to 2.5 nm was considered). Depending on the simulation results, the flexural rigidity values of F-actin for various loading rates are presented in Figure 7e. The average flexural rigidity obtained here was $(8.06 \pm 0.98) \times 10^{-26} \text{ Nm}^2$, which is comparable with reported values of the flexural rigidity in the range between 1.7×10^{-26} and $11 \times 10^{-26} \text{ Nm}^2$. Hi, 11, 12, 14, 15, 75 Besides, another well-known measure of polymer stiffness is persistence length (l_p). The equation to determine the persistent length of F-actin is $l_p = \frac{El}{k_b T}$, where T is the temperature (kelvin), and k_b is the Boltzmann constant. The measured average persistent length (l_p) of F-actin was $19.4 \pm 1.8 \, \mu\text{m}$, which is close to the findings of experimental investigations indicating a persistence length of F-actin 17.7 μm .

3.4. Torsional Deformation.

Due to its helical structure, an actin filament experiences longitudinal and torsional loads during interactions with myosin.⁷⁷ Hence, to understand the mechanism of force generation, it is essential to study F-actin's behavior under torsion. The actin filament's torsional rigidity can be measured based on its bending rigidity by assuming it as a homogeneous cylindrical rod.⁷⁸ However, due to the helical polymeric structures of F-actin, this assumption is a simplification. Molecular-level, fluctuation in the length of the filament, and the Brownian motions can be detected and observed. The phenomenon of equipartition of energy can be used to calculate F-actin's torsional rigidity by recording these fluctuations^{26, 29}. However, the computational time required to capture these fluctuations is significantly higher than the SMD simulations approach. We have used a user-defined forces SMD simulation protocol to determine the torsional rigidity of F-actin.

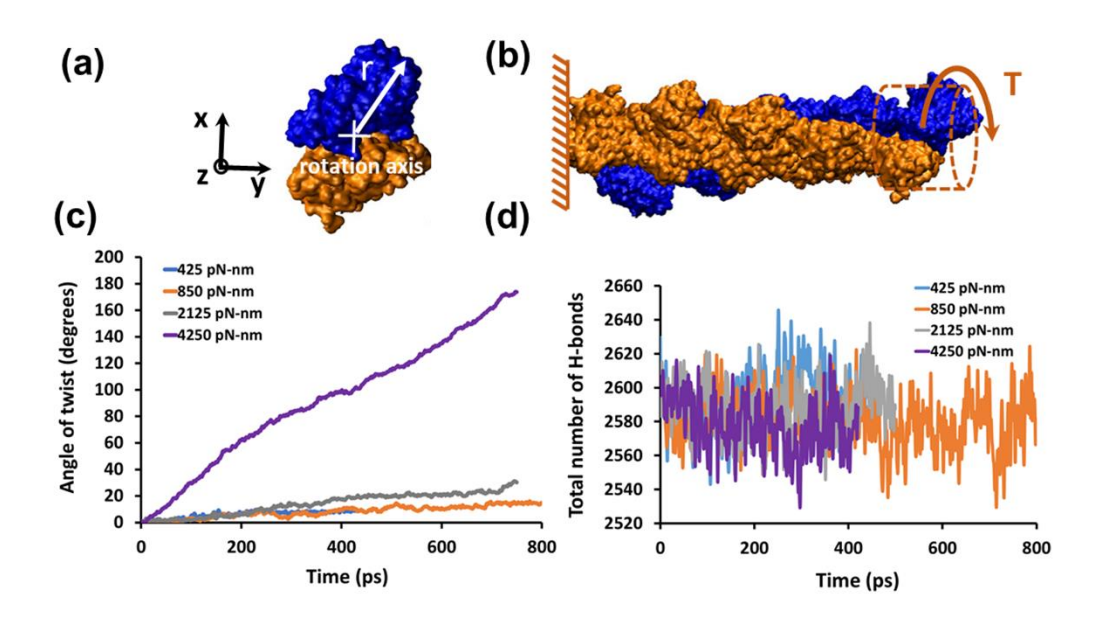


Figure 8. Schematic representation of the torsion test, angular displacement, hydrogen bond analysis. Images are showing a schematic arrangement of the torsion test setup. (a) The cross-sectional view of F-actin representing the rotational axis and radius. (b) The test setup showing toque (T) applied to one end of the filament. (c) Angular

displacement response of F-actin at different values of applied torque. Lower torque value resulted in smaller angular displacement, while higher values cause rapid and more significant angular displacement. All the values of torque induced twist gave nearly the same value of torsional rigidity. (d) There was no variation in the total number of hydrogen bonds observed for all sets of applied torques.

Torque is a moment that creates a twist in a structure to which it is applied. To set up the simulation, we fixed one end of an F-actin by applying constraints. The user-defined torque was applied on another end along the longitudinal axis to observe the angular deflection (twist). In the case of a prismatic shaft subjected to a constant torque, the torque-twist relationship is given by equation $\theta = \frac{Tl}{GI}$, where θ is the angle of twist, T is applied torque, l is the length of filament, G is shear modulus, and J is torsion constant (which depends on shafts cross-section, for circular crosssection = $\frac{\pi D^4}{32}$, where D is diameter). The F-actin structure is analogous with rod/shaft, hence by making use of the torque-twist relationship, the torsional rigidity was characterized. In a torquetwist relationship equation, the term G×J is called Torsional rigidity. The torque-twist relationship indicates that the angle of twist depends upon the magnitude of applied torque, length, and shear strength of filament. Similar results have been observed in the current SMD simulated torsion test of F-actin. Figure 8a-b represents schematic views of F-actin cross-section, an axis of rotation, and applied torque. The torque-twist responses of F-actin for different values of applied torque (T) are represented in figure 8c. It is observed that higher values of torque applied in the same time frame caused a higher and rapid growth of angular twist (θ) . This behavior is in agreement with the torque-twist relationship equation. Further, these results are used to quantify the Torsional rigidity of F-actin. Based on these simulation outcomes, we estimate the average torsional rigidity $GJ = (9.62 \pm 1.2) \times 10^{-26} \text{ Nm}^2$. The total number of hydrogen bonds in F-actin remained almost the same throughout the simulation (Figure 8d). Thus, the angular twist mechanism arises from the deformation of interlinked G-actin subunits and is not linked to breaking hydrogen bonds (Figure 8d).

4. CONCLUSIONS

In the present study, SMD simulations were performed to obtain detailed insight into the molecular mechanisms governing F-actin's deformation response. We have observed that elongation of F-actin comes at the cost of deformation of G-actin subunits and displacement of G-actin-G-actin interfaces, which gave rise to the formation of new noncovalent interactions. Elongation of F-actin initiated salt bridge formation between Lys113: Glu195 and Arg62: Glu270 at the inter-strand interfaces; these new connections increased inter-strand G-actin-G-actin bonding strength.

Further, we found that analogs to serrated locking plates, the contact between G-actin subunits at the inter-strand interfaces, provide resistance to their relative movement in longitudinal and directions, deformation. The intratransverse offering strength F-actin against strand interactions among G-actin subunits considerably contribute to filament strength because of their conformational arrangement and electrostatic, hydrophilic interactions. Hence, F-actin mechanics is controlled by conformational locks and nonbonded interaction energy at intra-strand and inter-strand G-actin interfaces. Elongation causing rotation of the free end depended on the extent of elongation and the strain rate-driven varying magnitude of rotation of G-actin subunits (3° to 7° per subunit). Further, we observed that F-actin's ability to carry axial compressive load arises from G-actin subunits' relatively stable configuration during compression. The influence of variation in strain rate on the mechanical properties of F-actin was investigated using SMD simulations. The obtained average values of Young's modulus = 1.95 ± 0.15 GPa, Flexural rigidity

(EI) = $(8.06 \pm 0.98) \times 10^{-26} \text{ Nm}^2$, Persistent length $(l_p) = 19.4 \pm 1.8 \, \mu\text{m}$, were found to be matching with existing experimental data. Here, the average compressive modulus found was 1.62 ± 0.18 GPa. Further, average torsional rigidity $GJ = (9.62 \pm 1.2) \times 10^{-26} \, \text{Nm}^2$ obtained from user-defined constant torque SMD simulation was found to be in close agreement with available experimental data, demonstrating the torsion test model's reliability. This research describes the mechanical response of an essential cellular protein, the F-actin, subjected to a wide range of conceivable loading paths and elucidates the fundamental mechanisms contributing to its resilience.

Supporting information

Definitions, details of the choice of the spring constant (Figures S1), details of the selection of the pulling velocities, details of the torsion test simulations, user-defined forces SMD simulation process (Figures S2), Steered Molecular Dynamics (SMD) parameters.

ACKNOWLEDGEMENTS

This work is made possible by the support of the National Science Foundation under NSF EPSCoR Track-1 Cooperative Agreement OIA #1946202 and the NDSU Grand Challenge funded Center for Engineered Cancer Testbeds. NSF grants #1229316 and #2019077 are acknowledged for the support of the computational resources at NDSU CCAST.

REFERENCES:

- 1. Bidone, T. C.; Kim, T.; Deriu, M. A.; Morbiducci, U.; Kamm, R. D., Multiscale impact of nucleotides and cations on the conformational equilibrium, elasticity and rheology of actin filaments and crosslinked networks. *Biomech. Model. Mechanobiol.* **2015**, 14, 1143-1155.
- 2. Dos Remedios, C. G.; Thomas, D. D., Molecular Interactions of actin: Actin structure and actin-binding proteins. *Springer Sci. & Bus. Media* **2012**, 32, 155–164.
- 3. Cooper, G. M.; Hausman, R. E., Structure and organization of actin filaments, In *The cell: Molecular approach*. 2nd Ed., Sinauer Associates. Sunderland, MA, **2004**, pp 473-496.
- 4. Blanchoin, L.; Boujemaa-Paterski, R.; Sykes, C.; Plastino, J., Actin dynamics, architecture, and mechanics in cell motility. *Physiol. Rev.* **2014**, 94, 235-263.
- 5. Alberts, B.; Johnson, A.; Lewis, J.; Raff, M.; Roberts, K.; Walter, P., The self-assembly and dynamic structure of cytoskeletal filaments. In *Molecular Biology of the Cell*. 4th Ed., Garland Science. **2002**, pp 2305-2355.
- 6. Fife, C. M.; McCarroll, J. A.; Kavallaris, M., Movers and shakers: cell cytoskeleton in cancer metastasis. *Br. J. Pharmacol.* **2014**, 171, 5507-5523.
- 7. Clarkson, E.; Costa, C. F.; Machesky, L. M., Congenital myopathies: diseases of the actin cytoskeleton. *J. Pathol.* **2004**, 204, 407-417.
- 8. Katti, D. R.; Katti, K. S.; Molla, S.; Kar, S., Biomechanics of Cells as Potential Biomarkers for Diseases: A New Tool in Mechanobiology. *Encycl. Biomed. Eng.* **2019**, 1-21.
- 9. Yallapu, M. M.; Katti, K. S.; Katti, D. R.; Mishra, S. R.; Khan, S.; Jaggi, M.; Chauhan, S. C., The roles of cellular nanomechanics in cancer. *Med. Res. Rev.* **2015**, 35, 198-223.
- 10. Suzuki, S.; Itakura, S.; Matsui, R.; Nakayama, K.; Nishi, T.; Nishimoto, A.; Hama, S.; Kogure, K., Tumor microenvironment-sensitive liposomes penetrate tumor tissue via attenuated interaction of the extracellular matrix and tumor cells and accompanying actin depolymerization. *Biomacromolecules* **2017**, 18, 535-543.
- 11. Isambert, H.; Venier, P.; Maggs, A. C.; Fattoum, A.; Kassab, R.; Pantaloni, D.; Carlier, M.-F., Flexibility of actin filaments derived from thermal fluctuations. Effect of bound nucleotide, phalloidin, and muscle regulatory proteins. *J. Biol. Chem.* **1995**, 270, 11437-11444.
- 12. Fujime, S., Quasi-elastic light scattering from solutions of macromolecules. II. Doppler broadening of light scattered from solutions of semi-flexible polymers, F-actin. *J. Phys. Soc. Jpn.* **1970**, 29, 751-759.
- 13. Nagashima, H.; Asakura, S., Dark-field light microscopic study of the flexibility of F-actin complexes. *J. Mol. Biol.* **1980**, 136, 169-182.
- 14. Takebayashi, T.; Morita, Y.; Oosawa, F., Electronmicroscopic investigation of the flexibility of Factin. *Biochim. Biophys. Acta, Protein Struct.* **1977**, 492, 357-363.
- 15. Gittes, F.; Mickey, B.; Nettleton, J.; Howard, J., Flexural rigidity of microtubules and actin filaments measured from thermal fluctuations in shape. *J. Cell Biol.* **1993**, 120, 923-934.
- 16. Gurmessa, B.; Ricketts, S.; Robertson-Anderson, R. M., Nonlinear actin deformations lead to network stiffening, yielding, and nonuniform stress propagation. *Biophys. J.* **2017**, 113, 1540-1550.
- 17. Rückerl, F.; Lenz, M.; Betz, T.; Manzi, J.; Martiel, J.-L.; Safouane, M.; Paterski-Boujemaa, R.; Blanchoin, L.; Sykes, C., Adaptive response of actin bundles under mechanical stress. *Biophys. J.* **2017**, 113, 1072-1079.
- 18. Majumdar, S.; Foucard, L. C.; Levine, A. J.; Gardel, M. L., Mechanical hysteresis in actin networks. *Soft matter* **2018**, 14, 2052-2058.
- 19. Lu, L.; Oswald, S. J.; Ngu, H.; Yin, F. C. P., Mechanical properties of actin stress fibers in living cells. *Biophys. J.* **2008**, 95, 6060-6071.

- 20. Chaudhuri, O.; Parekh, S. H.; Fletcher, D. A., Reversible stress softening of actin networks. *Nature* **2007**, 445, 295-298.
- 21. Kojima, H.; Ishijima, A.; Yanagida, T., Direct measurement of stiffness of single actin filaments with and without tropomyosin by in vitro nanomanipulation. *Proc. Natl. Acad. Sci. U. S. A.* **1994**, 91, 12962-12966.
- 22. Tsuda, Y.; Yasutake, H.; Ishijima, A.; Yanagida, T., Torsional rigidity of single actin filaments and actin—actin bond breaking force under torsion measured directly by in vitro micromanipulation. *Proc. Natl. Acad. Sci. U. S. A.* **1996**, 93, 12937-12942.
- 23. Kotila, T.; Kogan, K.; Enkavi, G.; Guo, S.; Vattulainen, I.; Goode, B. L.; Lappalainen, P., Structural basis of actin monomer re-charging by cyclase-associated protein. *Nat. Commun.* **2018**, 9, 1-12.
- 24. Splettstoesser, T.; Holmes, K. C.; Noé, F.; Smith, J. C., Structural modeling and molecular dynamics simulation of the actin filament. *Proteins: Struct., Funct., Bioinf.* **2011**, 79, 2033-2043.
- 25. Mehrafrooz, B.; Shamloo, A., Mechanical differences between ATP and ADP actin states: A molecular dynamics study. *J. Theor. Biol.* **2018**, 448, 94-103.
- 26. Shamloo, A.; Mehrafrooz, B., Nanomechanics of actin filament: A molecular dynamics simulation. *Cytoskeleton* **2018**, 75, 118-130.
- 27. Li, S.; Zhang, J.; Wang, C.; Nithiarasu, P., Atomistic Modeling of F-Actin Mechanical Responses and Determination of Mechanical Properties. *ACS Biomater. Sci. Eng.* **2018**, 4, 2794-2803.
- 28. Matsushita, S.; Inoue, Y.; Hojo, M.; Sokabe, M.; Adachi, T., Effect of tensile force on the mechanical behavior of actin filaments. *J. Biomech.* **2011**, 44, 1776-1781.
- 29. Matsushita, S.; Adachi, T.; Inoue, Y.; Hojo, M.; Sokabe, M., Evaluation of extensional and torsional stiffness of single actin filaments by molecular dynamics analysis. *J. Biomech.* **2010**, 43, 3162-3167.
- 30. Saunders, M. G.; Voth, G. A., Comparison between actin filament models: coarse-graining reveals essential differences. *Structure* **2012**, 20, 641-653.
- 31. Gong, B.; Wei, X.; Qian, J.; Lin, Y., Modeling and simulations of the dynamic behaviors of actin-based cytoskeletal networks. *ACS Biomater. Sci. Eng.* **2019**, 5, 3720-3734.
- 32. Janmey, P. A.; Euteneuer, U.; Traub, P.; Schliwa, M., Viscoelastic properties of vimentin compared with other filamentous biopolymer networks. *J. Cell. Biol.* **1991**, 113, 155-160.
- 33. Lee, H.; Eskin, S. G.; Ono, S.; Zhu, C.; McIntire, L. V., Force-history dependence and cyclic mechanical reinforcement of actin filaments at the single molecular level. *J. Cell Sci* **2019**, 132, jcs216911.
- 34. Strehle, D.; Mollenkopf, P.; Glaser, M.; Golde, T.; Schuldt, C.; Käs, J. A.; Schnauß, J., Single actin bundle rheology. *Molecules* **2017**, 22, 1804.
- 35. Shimozawa, T.; Ishiwata, S. i., Mechanical distortion of single actin filaments induced by external force: detection by fluorescence imaging. *Biophys. J.* **2009**, 96, 1036-1044.
- 36. Jégou, A.; Romet-Lemonne, G., Mechanically tuning actin filaments to modulate the action of actin-binding proteins. *Curr. Opin. Cell Biol.* **2020**, 68, 72-80.
- 37. Lee, C.-y.; Lou, J.; Wen, K.-k.; McKane, M.; Eskin, S. G.; Ono, S.; Chien, S.; Rubenstein, P. A.; Zhu, C.; McIntire, L. V., Actin depolymerization under force is governed by lysine 113: glutamic acid 195-mediated catch-slip bonds. *Proc. Natl. Acad. Sci. U. S. A.* 2013, 110, 5022-5027.
- 38. Leijnse, N.; Oddershede, L. B.; Bendix, P. M., Helical buckling of actin inside filopodia generates traction. *Proc. Natl. Acad. Sci. U. S. A.* **2015**, 112, 136-141.
- 39. Burla, F.; Mulla, Y.; Vos, B. E.; Aufderhorst-Roberts, A.; Koenderink, G. H., From mechanical resilience to active material properties in biopolymer networks. *Nat. Rev. Phys.* **2019**, 1, 249-263.
- 40. Ghosh, P.; Katti, D. R.; Katti, K. S., Mineral proximity influences mechanical response of proteins in biological mineral– protein hybrid systems. *Biomacromolecules* **2007**, 8, 851-856.
- 41. Pradhan, S. M.; Katti, K. S.; Katti, D. R., Structural hierarchy controls deformation behavior of collagen. *Biomacromolecules* **2012**, 13, 2562-2569.

- 42. Katti, D. R.; Ghosh, P.; Schmidt, S.; Katti, K. S., Mechanical properties of the sodium montmorillonite interlayer intercalated with amino acids. *Biomacromolecules* **2005**, 6, 3276-3282.
- 43. Ambre, A. H.; Katti, D. R.; Katti, K. S., Biomineralized hydroxyapatite nanoclay composite scaffolds with polycaprolactone for stem cell-based bone tissue engineering. *J. Biomed. Mater. Res., Part A* **2015**, 103, 2077-2101.
- 44. Ananthakrishnan, R.; Ehrlicher, A., The forces behind cell movement. *Int. J. Biol. Sci.* **2007**, 3, 303.
- 45. Ingber, D. E., Tensegrity I. Cell structure and hierarchical systems biology. *J. Cell Sci.* **2003**, 116, 1157-1173.
- 46. Ingber, D. E., Tensegrity II. How structural networks influence cellular information processing networks. *J. Cell Sci.* **2003**, 116, 1397-1408.
- 47. Galkin, V. E.; Orlova, A.; Salmazo, A.; Djinovic-Carugo, K.; Egelman, E. H., Opening of tandem calponin homology domains regulates their affinity for F-actin. *Nat. Struct. Mol. Biol.* **2010**, 17, 614.
- 48. Kabsch, W.; Mannherz, H. G.; Suck, D.; Pai, E. F.; Holmes, K. C., Atomic structure of the actin: DNase I complex. *Nature* **1990**, 347, 37-44.
- 49. Nelson, M. T.; Humphrey, W.; Gursoy, A.; Dalke, A.; Kalé, L. V.; Skeel, R. D.; Schulten, K., NAMD: a parallel, object-oriented molecular dynamics program. *Int. J. High Perform. Comput. Appl.* **1996**, 10, 251-268.
- 50. MacKerell Jr, A. D.; Bashford, D.; Bellott, M.; Dunbrack Jr, R. L.; Evanseck, J. D.; Field, M. J.; Fischer, S.; Gao, J.; Guo, H.; Ha, S., All-atom empirical potential for molecular modeling and dynamics studies of proteins. *J. Phys. Chem. B* **1998**, 102, 3586-3616.
- 51. Phillips, J. C.; Braun, R.; Wang, W.; Gumbart, J.; Tajkhorshid, E.; Villa, E.; Chipot, C.; Skeel, R. D.; Kale, L.; Schulten, K., Scalable molecular dynamics with NAMD. *J. Comput. Chem.* **2005**, 26, 1781-1802.
- 52. Zhang, Y.; Feller, S. E.; Brooks, B. R.; Pastor, R. W., Computer simulation of liquid/liquid interfaces. I. Theory and application to octane/water. *J. Chem. Phys.* **1995**, 103, 10252-10266.
- 53. Martyna, G. J.; Tobias, D. J.; Klein, M. L., Constant pressure molecular dynamics algorithms. *J. Chem. Phys.* **1994**, 101, 4177-4189.
- 54. Fujii, T.; Iwane, A. H.; Yanagida, T.; Namba, K., Direct visualization of secondary structures of Factin by electron cryomicroscopy. *Nature* **2010**, 467, 724-728.
- 55. Pollard, T. D.; Earnshaw, W. C.; Lippincott-Schwartz, J.; Johnson, G., In *Cell Biology*. Health Science (Elsevier) **2016**, pp 575-581.
- 56. Sano, K.-I.; Kawamura, R.; Tominaga, T.; Oda, N.; Ijiro, K.; Osada, Y., Self-repairing filamentous actin hydrogel with hierarchical structure. *Biomacromolecules* **2011**, 12, 4173-4177.
- 57. Xu, J.; Tseng, Y.; Wirtz, D., Strain Hardening of actin filament networks regulation by the dynamic cross-linking protein α-actinin. *J. Biol. Chem.* **2000**, 275, 35886-35892.
- 58. Fernández, P.; Pullarkat, P. A.; Ott, A., A master relation defines the nonlinear viscoelasticity of single fibroblasts. *Biophys. J.* **2006**, 90, 3796-3805.
- 59. Erk, K. A.; Henderson, K. J.; Shull, K. R., Strain stiffening in synthetic and biopolymer networks. *Biomacromolecules* **2010**, 11, 1358-1363.
- 60. Liu, X.; Pollack, G. H., Mechanics of F-actin characterized with microfabricated cantilevers. *Biophys. J.* **2002**, 83, 2705-2715.
- 61. Fixman, M.; Kovac, J., Polymer conformational statistics. III. Modified Gaussian models of stiff chains. *J. Chem. Phys.* **1973**, 58, 1564-1568.
- 62. MacKintosh, F. C.; Käs, J.; Janmey, P. A., Elasticity of semiflexible biopolymer networks. *Phys. Rev. Lett.* **1995**, 75, 4425.
- 63. Lorenzo, A. C.; Caffarena, E. R., Elastic properties, Young's modulus determination and structural stability of the tropocollagen molecule: a computational study by steered molecular dynamics. *J. Biomech.* **2005**, 38, 1527-1533.

- 64. Pradhan, S. M.; Katti, D. R.; Katti, K. S., Steered molecular dynamics study of mechanical response of full length and short collagen molecules. *J. Nanomech. Micromech.* **2011**, 1, 104-110.
- 65. Dupuis, D. E.; Guilford, W. H.; Wu, J.; Warshaw, D. M., Actin filament mechanics in the laser trap. *J. Muscle Res. Cell Motil.* **1997**, 18, 17-30.
- 66. Goldman, Y. E.; Huxley, A. F., Actin compliance: are you pulling my chain? *Biophys. J.* **1994**, 67, 2131.
- 67. Li, B.-l.; Wang, Y.-f.; Gong, J.-h., Using a form-finding model to analyze the effect of actin bundles on the stiffness of a cytoskeleton network. *J. Zhejiang Univ., Sci., A* **2014**, 15, 732-742.
- 68. Otterbein, L. R.; Graceffa, P.; Dominguez, R., The crystal structure of uncomplexed actin in the ADP state. *Science* **2001**, 293, 708-711.
- 69. Cozzone, A. J., Proteins: Fundamental chemical properties. In *Encyclopedia of Life Sciences*, John Wiley and Sons, Oxford, UK, **2010**, pp 1-9.
- 70. Jeffrey, G. A., In *An introduction to hydrogen bonding*. Oxford University Press, Oxford, UK, **1997**, 12, p 228.
- 71. Mattila, P. K.; Lappalainen, P., Filopodia: molecular architecture and cellular functions. *Nat. Rev. Mol. Cell Biol.* **2008**, 9, 446-454.
- 72. Mogilner, A.; Oster, G., Cell motility driven by actin polymerization. *Biophys. J.* **1996**, 71, 3030-3045.
- 73. Footer, M. J.; Kerssemakers, J. W. J.; Theriot, J. A.; Dogterom, M., Direct measurement of force generation by actin filament polymerization using an optical trap Proc. Natl. Acad. Sci. U. S. A. **2007**, 104, 2181-2186.
- 74. Dogterom, M.; Yurke, B., Measurement of the force-velocity relation for growing microtubules. *Science* **1997**, 278, 856-860.
- 75. Yoshino, S.; Umazume, Y.; Natori, R.; Fujime, S.; Chiba, S., Optical diffraction study of muscle fibers: II. Electro-optical properties of muscle fibers. *Biophys. Chem.* **1978**, 8, 317-326.
- 76. Buehler, M. J., Atomistic and continuum modeling of mechanical properties of collagen: elasticity, fracture, and self-assembly. *J. Mater. Res.* **2006**, 21, 1947-1961.
- 77. Nishizaka, T.; Yagi, T.; Tanaka, Y.; Ishiwata, S. i., Right-handed rotation of an actin filament in an in vitro motile system. *Nature* **1993**, 361, 269-271.
- 78. Yoshimura, H.; Nishio, T.; Mihashi, K.; Kinosita Jr, K.; Ikegami, A., Torsional motion of eosin-labeled F-actin as detected in the time-resolved anisotropy decay of the probe in the sub-millisecond time range. *J. Mol. Biol.* **1984**, 179, 453-467.

TABLE OF CONTENTS GRAPHIC

Dissociation Mechanisms of G-actin Subunits Govern Deformation Response of Actin Filament Sharad Jaswandkar, H M Nasrullah Faisal, Kalpana S. Katti, Dinesh R. Katti

